Research Article

Chan Lu, Zenghui Gou, Shan Li, Zhongao Mai, Xiaolong Li, and Yuhao Yang*

Superior photocatalytic degradation performance for gaseous toluene by 3D g-C_3N_4-reduced graphene oxide gels

https://doi.org/10.1515/gps-2022-0019
received August 13, 2021; accepted January 10, 2022

Abstract: Volatile organic compounds (VOCs) are major gaseous pollutants and one of the main causes of environmental problem, which can be extremely harmful to human health. Previous research has shown that photocatalytic oxidation is regarded as a promising technology to remove VOCs. However, for the time being, the photocatalytic performance in the field of removing VOCs by multiple reported photocatalysts cannot meet the demand of the practice. In this study, we have successfully synthesized a series of 3D gel composites with g-C_3N_4 (GC) and graphite oxide as precursors by a simple hydrothermal and freeze-drying method, which shows good photocatalytic degradation performance for gas toluene as model VOCs. The highest photocatalytic degradation ratio for gaseous toluene is about 86% in 180 min, which is about 3 times that of pure GC. The reason for the results is due to the strong adsorption capacity and very fast electrical conductivity of three dimensional (3D) reduced graphene oxide (RGO). This study implies that the 3D GC-RGO gels have potential usefulness for removing VOCs to meet the demand of the practice.

Keywords: VOCs, g-C_3N_4, reduced oxide graphene, 3D structure, photocatalytic degradation

1 Introduction

After mankind entered into 21st century, the environmental crisis faced by mankind has been growing on and on. Volatile organic compounds (VOCs) are major gaseous pollutants and one of the main causes of environmental crisis, which can be extremely harmful to human health [1]. The past 20 years have seen increasingly rapid advances in the field of removing VOCs using technologies, such as adsorption [2,3], catalysis [4–6], and photocatalysis [7–9], which have the potential to address the issue of environmental pollution [10–12]. Among these technologies, photocatalysis is regarded as a promising technology to remove VOCs due to its high catalytic activity, chemical stability, low-cost, and environmentally friendly property [13]. Up to now, many photocatalysts have been reported to remove VOCs, such as TiO_2, SnO_2, MnO_2, Bi_2WO_6, and so on [14–17]. However, for the time being, the photocatalytic performance in the field of removing VOCs by multiple reported photocatalysts cannot meet the demand of the practice because of the low utilization in the visible light as a result of wide band gap energy and high photogenerated charge recombination probability of the photocatalysts. Therefore, suitable photocatalyst should be investigated to overcome the disadvantages to meet the actual demand of removing VOCs.

Recently, there has been growing interest in graphitic carbon nitrides (g-C_3N_4; GC), a π-conjugated semiconductor, which is an emerging advanced photocatalyst in the field of hydrogen evolution via water splitting, photocatalytic CO_2 reduction, photodegradation of organic pollutants, and photodegradation of VOCs [18]. Compared to other common photocatalysts, GC has some advantages such as extraordinary visible light utilization efficiency because of its moderate bandgap energy (E_g = 2.7 eV), very simple synthesis method from cheap and available precursors, and high electronic conductivity as a result of unique conjugated structure. Nevertheless, the wider applications of the GC have been limited due to its high

* **Corresponding author: Yuhao Yang,** The School of Chemistry and Chemical Engineering, Shaanxi University of Science and Technology, Xi'an 710021, China, e-mail: yangyuhao@sust.edu.cn
Chan Lu, Zenghui Gou, Shan Li, Zhongao Mai: School of Architecture and Surveying and Mapping Engineering, Shaanxi Energy Institute, Xianyang 712000, China
Xiaolong Li: The School of Chemistry and Chemical Engineering, Shaanxi University of Science and Technology, Xi'an 710021, China

photogenerated charge recombination probability and low specific surface area, which is especially crucial in the field of photocatalytic degradation of VOCs [19].

Graphene (GR), a two-dimensional (2D) nanocarbon material, has been recently regarded as an ideal co-catalyst to enhance the photocatalytic efficiency of GC [20–23]. As a star electronic material which possesses superior charge mobility, it could be a platform to boost the photocatalytic efficiency of GC afterwards by accelerating photogenerated charge mobility. On the other hand, the large specific surface area of GR could also heighten the gas adsorption ability of GC, which can improve the photocatalytic activity in degrading VOCs. However, the 2D GR sheets should probably be aggregated or restacked during the wet chemistry synthesis, which would lower the electric conductivity [24]. To solve the above drawbacks, three-dimensional (3D) GR gels, a 3D cross-linked porous structure GR, has become an ideal candidate choice because its hierarchically porous structure achieved from GR sheets can maintain structural stability and expose more active sites from restraining the aggregation or restacking of GR sheets [25]. Zhang et al. prepared a 3D GC-TiO_2-GR aerogel composite, which possessed much higher visible light photocatalytic activity in the degradation of rhodamine B compared to the bare GC and TiO_2 due to the 3D porous structure of 3D GR with high surface areas and more active sites [26]. Tong et al. prepared a 3D porous GC/GR oxide aerogel as a high-efficient and visible-light responsive photocatalyst for degrading methyl orange in polluted water [27]. Zhang et al. synthesized 3D GR aerogel-GC metal-free heterojunctions for photodegrading organic dyes, which represent a superior efficiency [28]. Although some works have been done in the preparation and application of GC-3D GR gels, the research in removing VOCs using GC-3D GR gel composites have still not been reported as far as we know, which have great potentialities. Up to now, some previous works have been done in the preparation and application of GC-3D GR gels, but the current research have focused on the treatment of polluted water. There have been very few studies in removing VOCs using GC-3D GR gel composites as far as we know, which have great potentialities.

In this article, we have prepared a 3D GC-GR gel composites through a simple hydrothermal and freeze-drying method used as the precursor for removing gaseous toluene which is a model VOC. A series of 3D GC-reduced graphite oxide (3D GC-RGO) gels have been synthesized with various mass ratios between GC and graphite oxide (GO). Their photocatalytic efficiency in removing gaseous toluene was further investigated and the best mass ratio between GC and GO was found. In addition, the possible photocatalytic reaction mechanism was studied, and we hope our work could broaden the application of GC-based nanomaterials.

2 Experimental methods

2.1 Synthesis of samples

The GC and GO were synthesized by previously reported methods, which were calcination method and modified Hummers' method [29,30]. Then, the 3D GC-RGO gels were synthesized by a hydrothermal method and followed by freeze-drying. In detail, 100 mg GC was added to a 50 mL of mixed solvent of ethanol and water of 1:1 volume ratio and sonicated for 3 h to obtain a homogeneous solution. Then, 40 mg GO was added to a 20 mL of mixed solvent of ethanol and water also of 1:1 volume ratio and sonicated for 1 h to obtain a homogeneous solution. The GC solution and GO solution were mixed together and stirred for 1 h. Subsequently, the resulting solution was then transferred into a 100 mL Teflon-lined autoclave, and hydrothermally treated at 150°C for 12 h. In the hydrothermal process, the GO nanosheets were reduced to GR sheets which were described as RGO and the 3D hydrogel was formed by the co-assembly of GC nanosheets and RGO nanosheets. Finally, the 3D GC-RGO gels were obtained after washing with deionized water and freeze-drying. A series of 3D GC-RGO gels was synthesized by changing the mass ratio of GC to GO (m_{GC}:m_{GO} = 2, 1.5, 1, and 0.5) which are designated as GC-RGO-2, GC-RGO-1.5, GC-RGO-1, and GC-RGO-0.5, respectively.

2.2 Materials characterization

The X-ray diffraction (XRD) patterns were observed by D8 Advance Bruker X-ray diffractometer. The morphology of the prepared samples was observed by FEI Verios 460 scanning electron microscope (SEM). The X-ray photoelectron spectroscopy (XPS) analysis was done using Thermo Scientific K-Alpha. The UV-vis absorption spectra were measured by Shimadzu UV-2600.

2.3 Photocatalytic degradation of gas toluene (C_7H_8)

The photocatalytic degradation of C_7H_8 by the prepared samples was measured by a quartz photoreactor with 1 L

volume. 0.5 g photocatalyst was used in the measurement of the photocatalytic degradation. A 300 W visible light lamp was placed on the top of the photoreactor as the light source. The photoreactor was kept in dark for about 80 min before the irradiation to form adsorption equilibrium. The concentration of C_7H_8 in the reactor was analyzed by a gas chromatography. The initial concentration of C_7H_8 was of volume ratio of 1,000 ppm. The process schematic of the experimental system for toluene degradation is as shown in Figure 1.

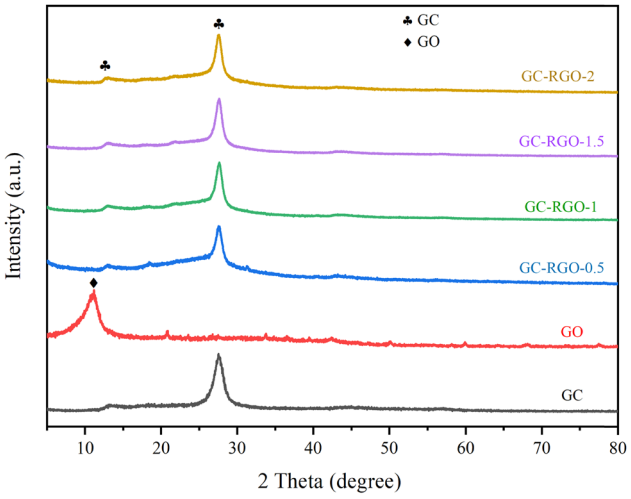

Figure 2: The XRD patterns of samples.

3 Results and discussion

3.1 Material characteristics

Figure 2 shows the XRD patterns of the prepared samples. There are two main peaks of GC at 12.9° and 27.5°, which indicate the (100) diffraction plane that relates to in-plane structural packing motif and (002) diffraction plane that relates to long-range inter planar stacking of aromatic systems [31]. Besides, only 1 peak at about 11° appears in the spectrum of GO pattern, which indicates the (002) reflection of GO [32]. For all GC-RGO samples, the peaks at 12.9° and 27.5° are clearly displayed, which demonstrate the preservation of GC in the composites. In addition, the peak at about 11° significantly disappeared for all GC-RGO samples, which indicates that the oxygen-containing functional groups of GO are reduced to RGO during hydrothermal process [33]. Moreover, the diffraction peak for RGO (002) at around 23.8° in all GC-RGO is negligible indicating that significant face-to-face stacking is absent as a result of presence of GC [34].

Figure 3 shows the XPS spectrum of GC-RGO-1.5 as a representative to investigate the surface chemical composition and chemical states. The survey spectrum displays the presence of C, N, and O elements in Figure 3a. The C 1s spectrum in Figure 3b can be divided into three peaks at 284.8, 286.3, and 288.7 eV, which are consistent with sp^2 C–C bond, C–O bond, and sp^2 N–C═N aromatic rings [35]. The presence of C–O bond represents the partial reduction of GO to RGO in the hydrothermal process. The N1s spectrum in the Figure 3c can be divided into four peaks at 398.6, 400.5, 401.5, and 404.4 eV, which are

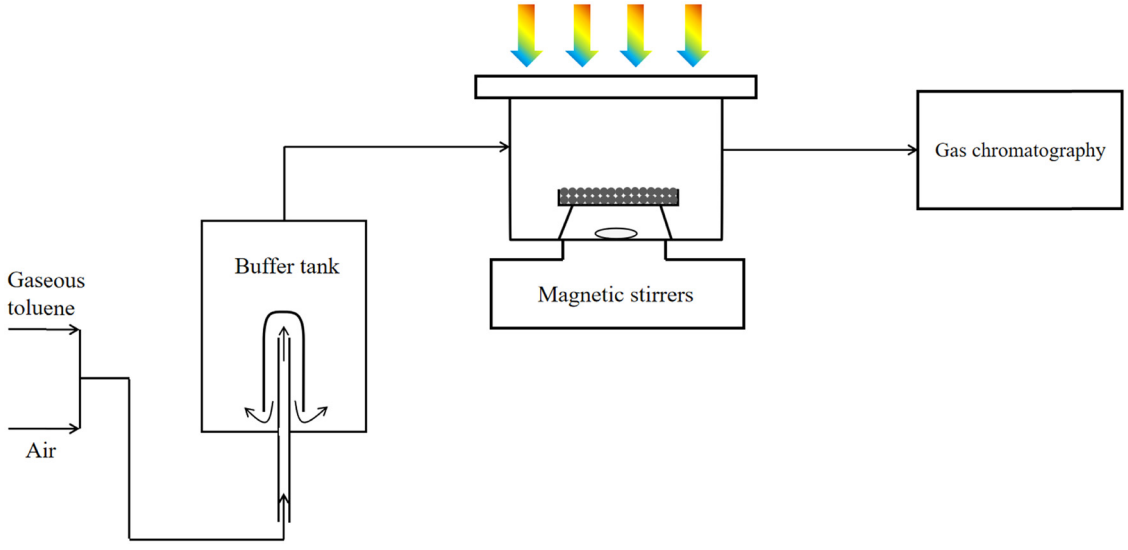

Figure 1: The process schematic of the experimental system for toluene degradation.

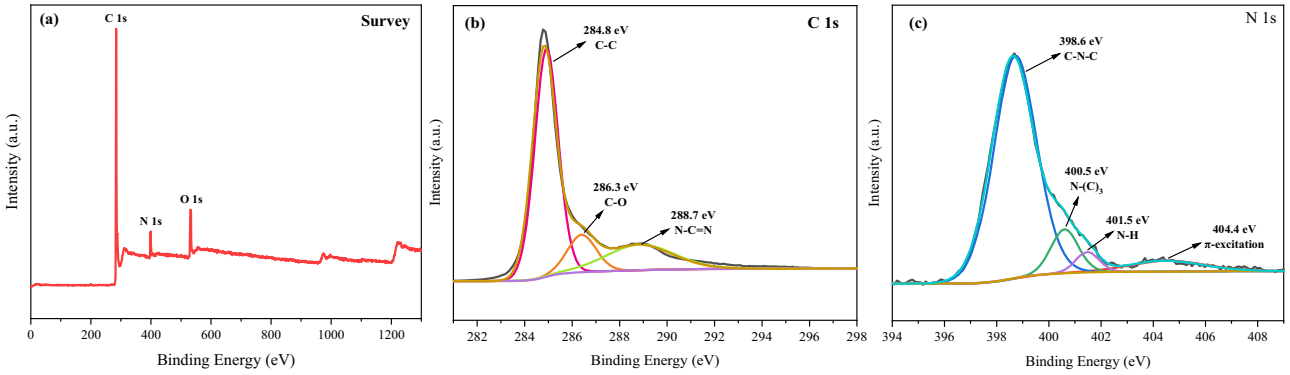

Figure 3: The XPS spectrum of GC-RGO-1.5: (a) survey, (b) C 1s, and (c) N 1s.

consistent with C–N–C, N–$(C)_3$, N–H functional group, and the π excitation in GC [35]. These peaks confirm the structure of GC in which heptazine heterocyclic ring units are the basic repeating unit. To further investigate the interaction of GC and RGO, the pure XPS spectrum of GC is also observed as shown in Figure 4. It can be seen that the typical peaks at C 1s and N1 s of GC-RGO-2 shift slightly compared with those of pure GC. In addition, the relative intensities of the two peaks at C1s are obviously changed. These results demonstrate the presence of chemical interaction between the GC and RGO.

The morphological characterization of samples is observed by SEM. Figure 5a shows the typical layered structure of pure GC. Figure 5b shows the specific 3D cross-linked porous structure assembled with 2D GR sheets, which have more specific surface area and active sites. Figure 5c shows the morphology of GC-RGO-1.5 and Figure 5d shows the partial enlarged detail of Figure 5c. It can be seen that the typical layered GC was loaded in the interior and surface of 3D porous RGO. In this particular structure, the 3D RGO acts as a supporter for GC. The results of SEM demonstrate that the GC and 3D RGO are successfully combined by the hydrothermal method.

To investigate the optical properties of the samples, the UV-Vis diffuse reflectance spectrum (DRS) spectra were observed as shown in Figure 6. It can be seen that the absorption edge of pure GC is around 450 nm, which is greater than the common reported photocatalysts in the visible region to remove VOCs such as TiO_2, SnO_2, and so on. Meanwhile, a strong absorption intensity in the full spectrum especially in visible region of all GC-RGO samples are observed, which indicates that the 3D RGO has good visible absorption ability. The impressive visible absorption ability of 3D RGO is due to the internal light scattering process in its 3D porous structure [36]. Additionally, the absorption intensity decreases, and the absorption edge shifts blue slightly as the amount of GC increases in the GC-RGO samples. It can be explained as the more the

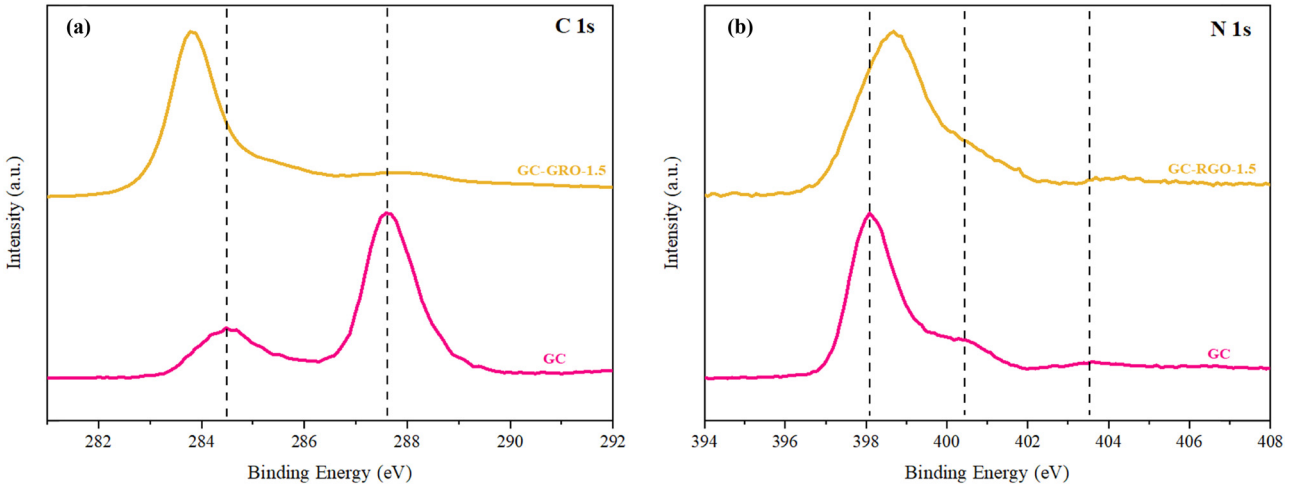

Figure 4: The XPS spectrum of GC and GC-RGO-1.5: (a) C 1s and (b) N 1s.

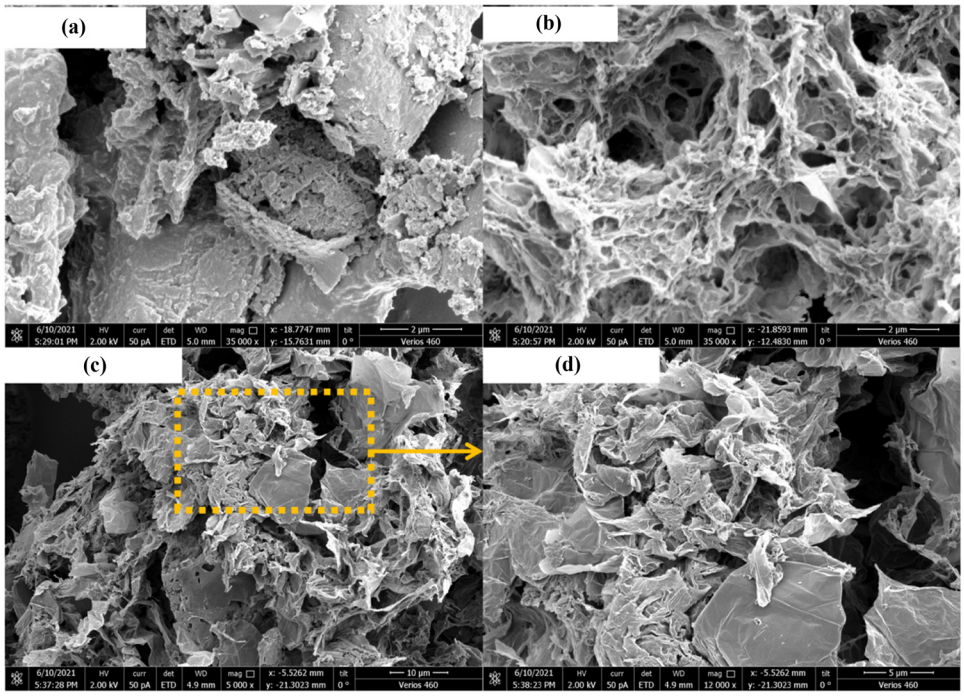

Figure 5: The SEM image of samples: (a) GC, (b) 3D RGO, and (c and d) GC-RGO-1.5.

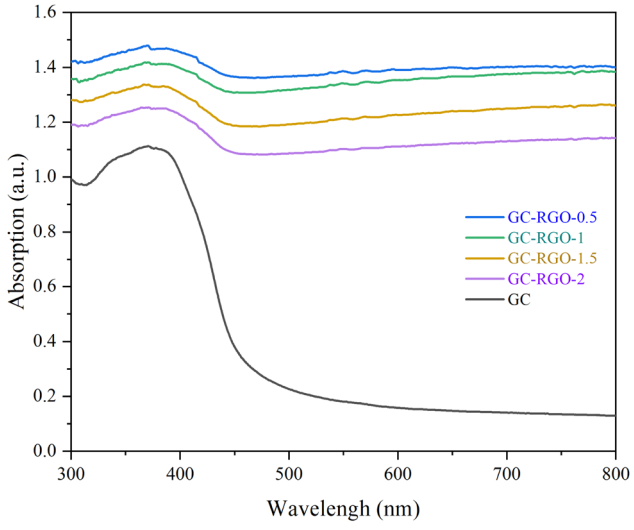

Figure 6: The UV-Vis DRS of samples.

mass ratio of GC to 3D RGO, the result is more likely to pristine GC. These results indicate that the composites of GC and 3D RGO can enhance the light absorption of pristine GC, which could accelerate the generation of electron-hole pairs, thereby improve the photocatalytic activity of GC.

3.2 Photocatalytic activity for gaseous toluene

Figure 7 displays the photocatalytic activity of the prepared samples for gaseous toluene. In Figure 7, the C_0 represented the initial concentration of C_7H_8 when pollutants were added in the reactor at 0 min, and the C was

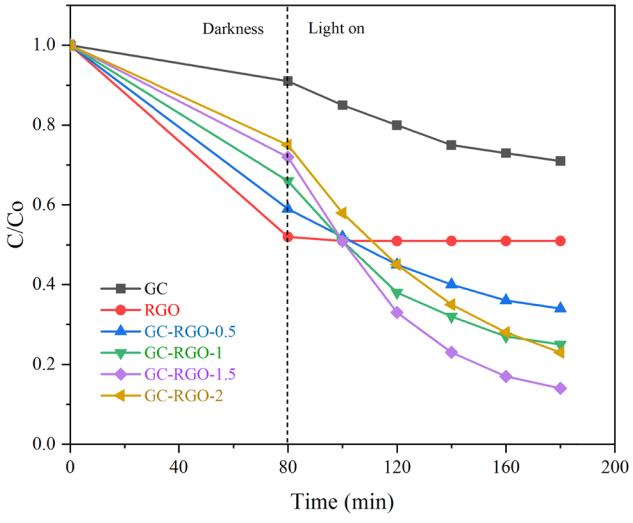

Figure 7: Removal efficiency for gaseous toluene.

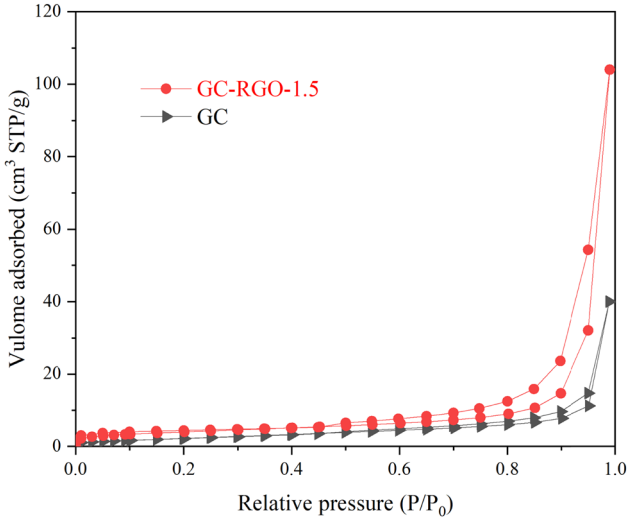

Figure 8: Nitrogen adsorption–desorption isotherms of GC and GC-RGO-1.5.

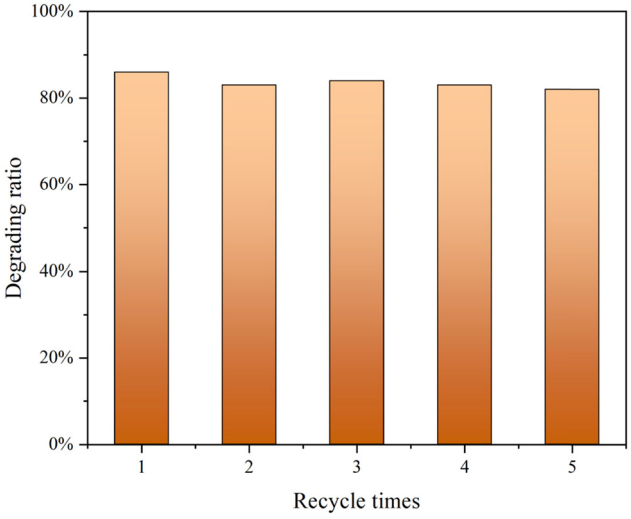

Figure 9: Photocatalytic stability in the removal of gaseous toluene by GC-RGO-1.5.

the measured concentration of remaining toluene at different time in the reactor. In the dark condition (first 80 min), the numerical value of C/C_0 reflects the adsorption ability of the prepared samples. When the adsorption equilibrium is reached, pure GC reflects the weakest adsorption capacity and pure 3D RGO reflects the strongest adsorption capacity because the specific surface area of 3D RGO is big relative to GC [28]. On the other hand, the adsorption capacity of GC-RGO samples increases with the decrease in GC, which is also because of the above reason. Figure 8 displays the nitrogen adsorption/desorption isotherms of the obtained samples. The calculated specific surface area of GC-RGO-1.5 (55.7 $cm^2 \cdot g^{-1}$) is about 1.67 times bigger than that of GC (33.5 $cm^2 \cdot g^{-1}$), which explains the above results.

When the light is on, the concentration of C_7H_8 rapidly decreases for all the prepared samples except pure 3D RGO, because of its non-photocatalytic ability. What is noteworthy is that there is an optimal mass ratio of GC to RGO for photocatalytic removal efficiency of gaseous toluene. The GC-RGO-1.5 has the highest photocatalytic degradation ratio for gaseous toluene, which is about 86% in 180 min. There may be two reasons: (1) Superfluous GC can influence the uniformity of dispersion in the 3D RGO which leads to aggregation of GC and the increase in the recombination of photogenerated electron-hole pairs; (2) The specific surface area of GC-RGO samples decreases with the decrease in RGO, which decreases the adsorption capacity and reduces the number of active sites. In addition, the photocatalytic degradation ratio of the prepared samples was stable across the five replicates of the experiment, as shown in Figure 9.

3.3 The photocatalytic degradation mechanism for gaseous toluene

As is well known, the band gap can be estimated with a linear fit to the plot of the square root of Kubelka-Munk function against hν of the light. As shown in Figure 10a, the band gap of GC is estimated to be 2.84 eV. Additionally, the valence band (VB) of GC is estimated to be 1.74 eV from the XPS VB energy spectrum which is shown in Figure 10b. So, the conduction band (CB) of GC is −1.1 eV (E_g = VB − CB). In addition, the photoluminescence (PL) spectra of pure GC and GC-RGO-1.5 with 365 nm excitation wavelength are shown in Figure 11. The PL spectrum of GC-RGO-1.5 is quenched relative to pure GC, indicating that the recombination of the photo-induced electron-hole was limited. This result is attributed to the improved charge transfer from GC to RGO.

Based on these results, the photocatalytic degradation mechanism for gaseous toluene is schematically illustrated in Figure 12. Under visible light irradiation, GC can be excited to generate electron-hole pairs. The electron can easily transfer to the RGO due to the very fast electrical conductivity and 3D framework of RGO, which can reduce the recombination of photogenerated electron-hole pairs thus promoting the photocatalytic activity.

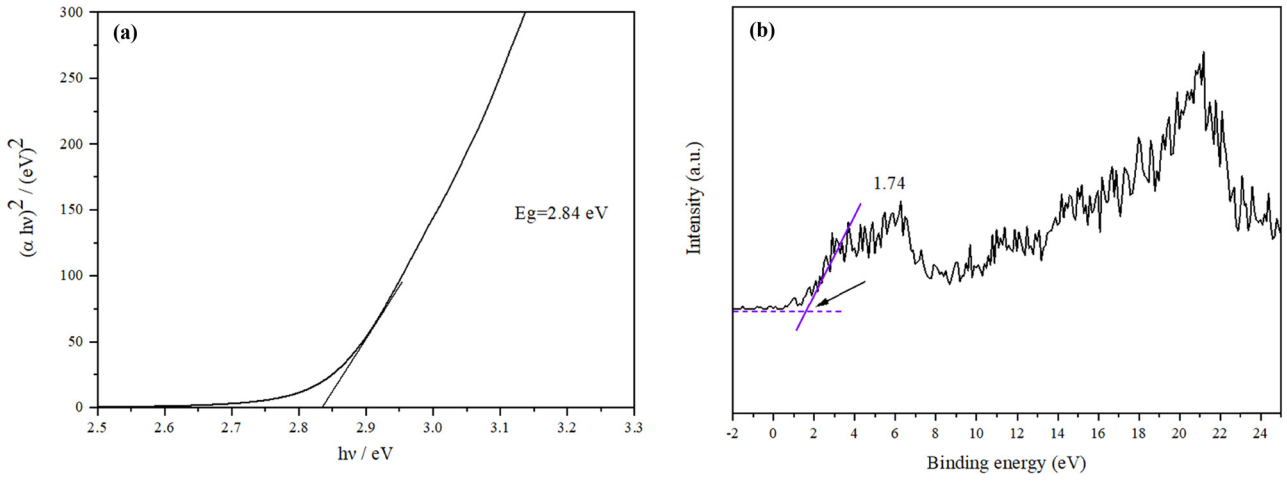

Figure 10: (a) Spectrum expressed as the Kubelka-Munk function and (b) the VB energy spectrum of GC.

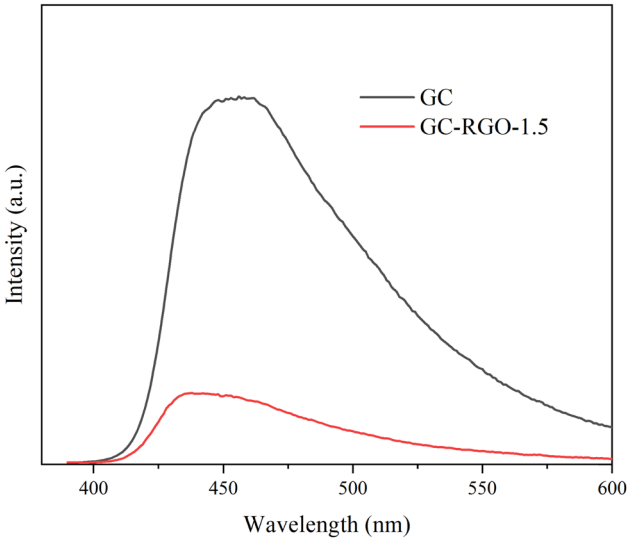

Figure 11: PL spectra of GC and GC-RGO-1.5.

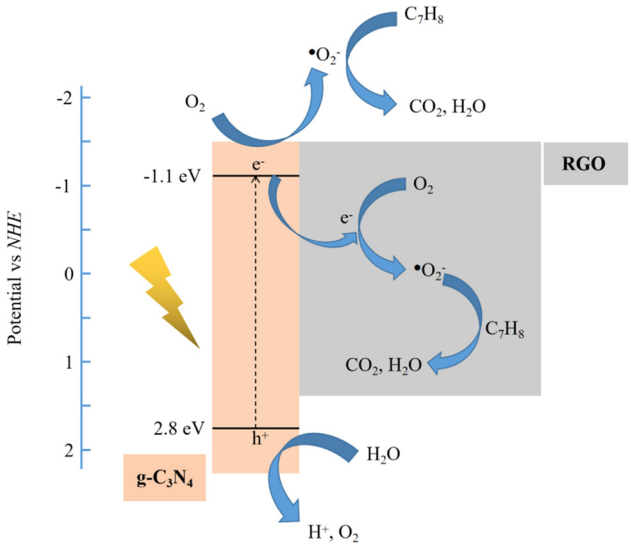

Figure 12: The photocatalytic degradation mechanism for gaseous toluene.

Then, O_2^- is generated on the surface of RGO and CB band of GC simultaneously by the generated electron reacting with O_2. Furthermore, the C_7H_8 has been degraded to CO_2 and H_2O by reacting with O_2^-.

4 Conclusion

In summary, we have successfully synthesized a series of 3D framework composites with GC and GO as precursors by a simple hydrothermal and freeze-drying method. The 3D GC-RGO nanocomposites show good photocatalytic degradation performance for C_7H_8 compared to pure GC. The reason for the results is due to the strong adsorption capacity and very fast electrical conductivity of 3D RGO. And it is worth noting that there is an optimal mass ratio of GC to GO for photocatalytic removal efficiency of gaseous toluene, which is 1.5 times mass ratio of GC relative to GO. The photocatalytic degradation mechanism for gaseous toluene have also been discussed. These findings highlight the potential usefulness of 3D GC-RGO nanocomposites in the field of photocatalytic removal of VOCs, which expand the application scope of 3D GR as co-photocatalyst.

Funding information: This work was supported by the Scientific Research Project of Shaanxi Energy Institute

(19KYP02) and Shaanxi Natural Science Basic Research Program (2021JQ-533).

Author contributions: Chan Lu: writing – original draft, writing – review and editing, methodology, and formal analysis; Zenghui Gou: writing – original draft and formal analysis; Shan Li: methodology and data curation; Zhongao Mai: methodology; Xiaolong Li: methodology; Yuhao Yang: writing – review and editing.

Conflict of interest: Authors state no conflict of interest.

Data availability statement: All data generated or analyzed during this study are included in this published article.

References

[1] Zou W, Gao B, Ok YS, Dong L. Integrated adsorption and photocatalytic degradation of volatile organic compounds (VOCs) using carbon-based nanocomposites: a critical review. Chemosphere. 2019;218:845–59.

[2] Zhang XD, Shi XY, Zhao QY, Li YT, Wang JF, Yang Y, et al. Defects controlled by acid-modulators and water molecules enabled UiO-67 for exceptional toluene uptakes: an experimental and theoretical study. Chem Eng J. 2022;427:131573.

[3] Shi XY, Zhang XD, Bi FK, Zheng ZH, Sheng LJ, Xu JC, et al. Effective toluene adsorption over defective UiO-66-NH_2: an experimental and computational exploration. J Mol Liq. 2020;316:113812.

[4] Wang Y, Wang C, Zeng K, Wang S, Zhang H, Li X, et al. Revealing the strong interaction effect of MnO_x nanoparticles and Nb_2O_5 supports with variable morphologies on catalytic propane oxidation. Appl Surf Sci. 2021;5:151797.

[5] Bi F, Zhang X, Chen J, Yang Y, Wang Y. Excellent catalytic activity and water resistance of UiO-66-supported highly dispersed Pd nanoparticles for toluene catalytic oxidation. Appl Cata B Env. 2020;15:118767.

[6] Feng J, Yao T, Chu C, Ma Z, Han H. Proton-responsive annunciator based on I-motif DNA structure modified metal organic frameworks for ameliorative construction of electrochemical immunosensing interface. J Coll Inter Sci. 2021;608:2050–7.

[7] Yue K, Zhang X, Jiang S, Chen J, Yang Y, Bi F, et al. Recent advances in strategies to modify MIL-125 (Ti) and its environmental applications. J Mol Liq. 2021;335:116108.

[8] Zhang X, Chen J, Jiang S, Zhang X, Bi F, Yang Y, et al. Enhanced photocatalytic degradation of gaseous toluene and liquidus tetracycline by anatase/rutile titanium dioxide with heterophase junction derived from materials of institut lavoisier-125 (Ti): degradation pathway and mechanism studies. J Coll Inter Sci. 2021;588:122–37.

[9] Chen J, Zhang X, Shi X, Bi F, Yang Y, Wang Y. Synergistic effects of octahedral TiO_2-MIL-101 (Cr) with two heterojunctions for enhancing visible-light photocatalytic degradation of liquid tetracycline and gaseous toluene. J Coll Inter Sci. 2020;579:37–49.

[10] Ahmed SN, Haider W. Heterogeneous photocatalysis and its potential applications in water and wastewater treatment: a review. Nanotechnology. 2018;29(34):342001.

[11] Wenderich K, Mul G. Methods, mechanism, and applications of photodeposition in photocatalysis: a review. Chem Rev. 2016;116(23):14587–619.

[12] Boyjoo Y, Sun H, Liu J, Pareek VK, Wang S. A review on photocatalysis for air treatment: from catalyst development to reactor design. Chem Eng J. 2017;310:537–59.

[13] Suárez S, Jansson I, Ohtani B, Sánchez B. From titania nanoparticles to decahedral anatase particles: photocatalytic activity of TiO_2/Zeolite hybrids for VOCs oxidation. Cata Today. 2019;326:2–7.

[14] Tobaldi DM, Dvoranová D, Lajaunie L, Rozman N, Figueiredo B, Seabra MP, et al. Graphene-TiO_2 hybrids for photocatalytic-aided removal of VOCs and nitrogen oxides from outdoor environment. Chem Eng J. 2021;405:126651.

[15] Li X, Li J, Zhang G, Yang W, Yang L, Shen Y, et al. Enhanced reactant activation and transformation for efficient photocatalytic acetone degradation on SnO_2 via Hf doping. Adv Sustain Syst. 2021;5(8):2100115.

[16] Wu P, Dai S, Chen G, Zhao S, Xu Z, Fu M, et al. Interfacial Effects in Hierarchically Porous α-MnO_2/Mn_3O_4 heterostructures promote photocatalytic oxidation activity. Appl Catal B Env. 2020;268:118418.

[17] Liu Y, Zhou Y, Tang Q, Li Q, Chen S, Sun Z, et al. A direct Z-scheme Bi_2WO_6/NH_2-UiO-66 nanocomposite as an efficient visible-light-driven photocatalyst for NO removal. RSC Adv. 2020;10(3):1757–68.

[18] Naseri A, Samadi M, Pourjavadi A, Moshfegh AZ, Ramakrishna S. Graphitic carbon nitride (g-C_3N_4)-based photocatalysts for solar hydrogen generation: recent advances and future development directions. J Mater Chem A. 2017;5(45):23406–33.

[19] Meng J, Wang X, Yang X, Hu A, Guo Y, Yang Y. Enhanced gas-phase photocatalytic removal of aromatics over direct Z-scheme-dictated $H_3PW_{12}O_{40}$/g-C_3N_4 film-coated optical fibers. Appl Catal B Env. 2019;251:168–80.

[20] Moradi S, Isari AA, Hayati F, Kalantary RR, Kakavand B. Co-implanting of TiO_2 and liquid-phase-delaminated g-C_3N_4 on multi-functional graphene nanobridges for enhancing photocatalytic degradation of acetaminophen. Chem Eng J. 2021;414:128618.

[21] Liu J, Wei X, Sun W, Guan X, Zheng X, Li J. Fabrication of S-scheme CdS-g-C_3N_4-graphene aerogel heterojunction for enhanced visible light driven photocatalysis. Environmen Res. 2021;197:111136.

[22] Li J, Yu X, Zhu Y, Fu X, Zhang Y. 3D-2D-3D BiOI/Porous g-C_3N_4/graphene hydrogel composite photocatalyst with synergy of adsorption-photocatalysis in static and flow systems. J Alloy Compd. 2021;850:156778.

[23] Jiang J, Duan D, Ma J, Jiang Y, Long R, Gao C, et al. Van der Waals heterostructures by single cobalt sites-anchored graphene and g-C_3N_4 nanosheets for photocatalytic syngas production with tunable CO/H_2 ratio. Appl Catal B Env. 2021;295:120261.

[24] Xin X, Li SH, Zhang N, Tang ZR, Xu YJ. 3D Graphene/AgBr/Ag cascade aerogel for efficient photocatalytic disinfection. Appl Cataly B Env. 2019;245:343–50.
[25] Xie X, Zhang N, Tang ZR, Xu YJ. An adaptive geometry regulation strategy for 3D graphene materials: towards advanced hybrid photocatalysts. Chem Sci. 2018;9(47):8876–82.
[26] Zhang JJ, Fang SS, Mei JY, Zheng GP, Zheng XC, Guan XX. High-efficiency removal of rhodamine B dye in water using g-C_3N4 and TiO_2 co-hybridized 3D graphene aerogel composites. Sep Purif Technol. 2018;194:96–103.
[27] Tong Z, Yang D, Shi J, Nan Y, Sun Y, Jiang Z. Three-dimensional porous aerogel constructed by g-C_3N_4 and graphene oxide nanosheets with excellent visible-light photocatalytic performance. ACS Appl Mater Inter. 2015;7(46):25693–701.
[28] Zhang JY, Zhang SH, Li J, Zheng XC, Guan XX. Constructing of 3D graphene aerogel-g-C_3N_4 metal-free heterojunctions with superior purification efficiency for organic dyes. J Mol Liq. 2020;310:113242.
[29] Yang YH, Lu C, Ren J, Li X, Ma YN, Huang WH, et al. Enhanced photocatalytic hydrogen evolution over TiO_2/g-C_3N_4 2D heterojunction coupled with plasmon Ag nanoparticles. Ceram Inter. 2020;46(5):5725–32.
[30] Yang YH, Liu EZ, Dai HZ, Kang LM, Wu HT, Fan J, et al. Photocatalytic activity of Ag-TiO_2-graphene ternary nanocomposites and application in hydrogen evolution by water splitting. Inter J Hydro Eng. 2014;39(15):7664–71.
[31] Yang YH, Li XL, Lu C, Huang WH. G-C_3N_4 nanosheets coupled with TiO_2 nanosheets as 2D/2D heterojunction photocatalysts toward high photocatalytic activity for hydrogen production. Catal Lett. 2019;149:2930–9.
[32] Zhang R, Huang Z, Li C, Zuo Y, Zhou Y. Monolithic G-C_3N_4/reduced graphene oxide aerogel with *in situ* embedding of Pd nanoparticles for hydrogenation of CO_2 to CH_4. Appl Sur Sci. 2019;475:953–60.
[33] Jo WK, Kumar S, Eslava S, Tonda S. Construction of Bi_2WO6/RGO/g-C_3N_4 2D/2D/2D hybrid Z-scheme heterojunctions with large interfacial contact area for efficient charge separation and high-performance photoreduction of CO_2 and H_2O into solar fuels. Appl Cataly B Env. 2018;239:586–98.
[34] Si YC, Samulski ET. Exfoliated graphene separated by platinum nanoparticles. Chem Mater. 2008;20:6792–7.
[35] Wu Y, Fu CF, Huang Q, Zhang P, Cui P, Ran J, et al. 2D Heterostructured nanofluidic channels for enhanced desalination performance of graphene oxide membranes. ACS Nano. 2021;15(4):7586–95.
[36] Zhang F, Li YH, Li JY, Tang ZR, Xu YJ. 3D Graphene-based gel photocatalysts for environmental pollutants degradation. Environ Pollut. 2019;253:365–76.